

TiO₂/LiCl-Based Nanostructured Thin Film for Humidity Sensor Applications

Andrii I. Buvailo,^{†,‡} Yangjun Xing,[†] Jacqueline Hines,[§] Norman Dollahon,[⊥] and Eric Borguet*,^{†,‡}

[†]Department of Chemistry, Temple University, Philadelphia, Pennsylvania 19122, United States

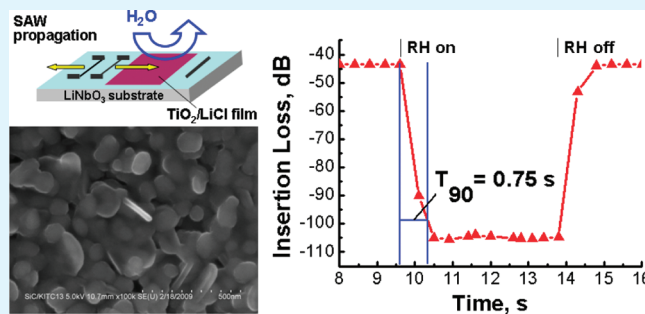
[‡]Department of Chemistry, Kyiv National Taras Shevchenko University, Kyiv, Ukraine 01033

[§]Applied Sensor Research and Development Corporation, Arnold, Maryland 21012, United States

[⊥]Department of Biology, Villanova University, Villanova, Pennsylvania, United States

 Supporting Information

ABSTRACT: A simple and straightforward method of depositing nanostructured thin films, based on LiCl-doped TiO₂, on glass and LiNbO₃ sensor substrates is demonstrated. A spin-coating technique is employed to transfer a polymer-assisted precursor solution onto substrate surfaces, followed by annealing at 520°C to remove organic components and drive nanostructure formation. The sensor material obtained consists of coin-shaped nanoparticles several hundred nanometers in diameter and less than 50 nm thick. The average thickness of the film was estimated by atomic force microscopy (AFM) to be 140 nm. Humidity sensing properties of the nanostructured material and sensor response times were studied using conductometric and surface acoustic wave (SAW) sensor techniques, revealing reversible signals with good reproducibility and fast response times of about 0.75 s. The applicability of this nanostructured film for construction of rapid humidity sensors was demonstrated. Compared with known complex and expensive methods of synthesizing sophisticated nanostructures for sensor applications, such as physical vapor deposition (PVD) and chemical vapor deposition (CVD), this work presents a relatively simple and inexpensive technique to produce SAW humidity sensor devices with competitive performance characteristics.



KEYWORDS: humidity sensors, surface acoustic wave, titanium dioxide, thin films, lithium chloride

INTRODUCTION

The creation of reliable sensors for monitoring humidity is an important task for ensuring appropriate atmospheric conditions at agricultural, medical, and industrial facilities as well as maintaining comfort in buildings.^{1–3} A number of criteria such as high sensitivity, repeatability, and short response time are generally required for such devices.^{4–6} It should be noted that for specific uses, such as meteorology applications (in radiosondes and weather balloons⁷), medical diagnostics of exhaled air (for example, pulmonary function diagnosis⁸), and aerospace applications on board of space vehicles,⁹ the response time becomes crucial because humidity measurements and data acquisition in such cases are to be conducted in real time.

The preparation of novel materials with potential humidity-sensitive properties is a key process in the development of new humidity sensors. There are several types of materials which are generally used as the sensitive layer of humidity sensor devices, the most common being polymers and ceramics.^{10,11} Both types of materials usually operate via a proton conduction mechanism: water condenses on the surface of materials to form aquatic layers that allow protons to migrate throughout the sensor

surface to produce a specific sensor conductivity via a Grotthuss mechanism.¹⁰ In order to regulate protonic conductivity with the aim of increasing sensor sensitivity and expanding the region of measurable relative humidity (RH), some additives are usually introduced into sensor materials, in particular, alkali ions.^{10,12,13} While it is technically easier to deposit polymers on the surface of sensor substrates, because it does not require annealing at high temperature as in the case of ceramic substrates, polymeric layers usually can not operate at increased temperatures and high RH. Besides, many polymer sensors exhibit substantial drift with time due to degradation of polymer layers upon exposure to high humidity and some air components, such as CO₂.¹⁴

In contrast, ceramic materials based on various metal oxides appear to be advantageous over polymeric materials, as they possess high chemical and mechanical stability, high sensitivity, and generally faster response dynamics compared to polymer materials.^{15,16} Among the most popular ceramic type materials used for measuring

Received: November 13, 2010

Accepted: December 16, 2010

Published: February 1, 2011

humidity are oxides such as Al_2O_3 ,^{10,17,18} TiO_2 ,^{10,17,19} SiO_2 ,^{10,17} and ZnO ^{3,10,20} and various spinel compounds.¹⁰ In the work described in this paper, we chose titanium dioxide as a base for creating our humidity sensing film. TiO_2 -based materials containing different dopants are widely used for creation of humidity sensors.^{13,21,22} Examples include TiO_2 ceramics doped with various concentrations of LiCl and KCl which make the films more conductive and more sensitive to moisture. For instance, it was reported that 1–10% doping by the above salts improves the sensitivity of humidity sensors by several orders of magnitude.^{23,24} Especially responsive and stable LiCl-doped TiO_2 sensors were fabricated by Li et al., which showed outstanding sensitivity and fast response due to formation of 1D nanofibers possessing high surface-to-volume ratio.²⁴

It is important to note that the morphology of the sensor material plays a substantial role in the overall sensor performance.^{19,20,25} A number of different nanostructures were studied with respect to humidity sensing,²⁰ such as nanowires,^{26,27} nanorods,^{19,20,27} nanobelts,²⁷ and nanotrapods,²⁸ together with more usual round shaped nanoparticles²⁹ and meso-pore materials.³⁰ However, increasing the functionality of the material by controlling shape and arrangement of nanoparticles usually requires sophisticated and expensive deposition techniques, such as chemical vapor deposition (CVD), physical vapor deposition (PVD), magnetron sputtering, pulsed laser deposition, etc.^{17,18,25,31–33} For example, it was reported that a highly organized Al_2O_3 -based nanomaterial, deposited by glancing angle deposition (GLAD, which is a modified PVD deposition technique offering the possibility to control morphology on a 10 nm scale), is able to detect humidity change on a millisecond time scale, which is one of the fastest humidity sensor responses reported to date.³³ Single SnO_2 nanowires were obtained by a CVD technique and revealed high sensitivity to relative humidity.²⁵ The main disadvantages of sensors utilizing such materials for high volume applications are the need for extensive additional development to achieve reproducible process techniques suitable for implementation in a manufacturing environment and the increased cost of the sensors that would result from the use of expensive equipment in production (CVD, PVD, etc.). Thus, the development of a nanostructured, humidity sensitive film compatible with standard, low complexity manufacturing procedures is of great practical interest for low-cost humidity sensor fabrication.

In this paper, we report the synthesis of a TiO_2 -based nanomaterial doped with LiCl, which was deposited on glass and LiNbO_3 sensor substrates by spin-coating with subsequent annealing at elevated temperature, and a study of the humidity sensing properties of these devices using conductometric and surface acoustic wave (SAW) sensor techniques. The synthetic approach used in this work led to the formation of TiO_2 -based films with unusual coin-shaped morphology as was demonstrated by scanning electron microscopy (SEM). The conductometric and SAW sensors produced were tested at varying relative humidity levels, and it was found that both types of sensor respond rapidly, in less than one second, with complete response reversibility. Hence, the films reported here are applicable for use in both conductometric and SAW humidity sensors. While there are reports of conductometric sensors exhibiting much faster response dynamics and higher sensitivity, the SAW sensor obtained in this work appears to be among the fastest SAW humidity sensors reported to date with response and recovery times of 0.75 and 1 s, respectively. When the advantages of SAW technology to provide easily realizable wireless and batteryless operation modes are

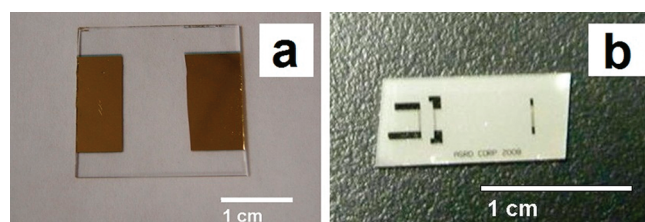


Figure 1. Sensor substrates used for creating conductometric (a) and SAW (b) humidity sensors.

taken into account, the SAW humidity sensor presented in this work appears to be potentially very useful in situations when real time humidity measurement is needed in areas of difficult access, where wired connections would be problematic, and in applications where the use of battery powered wireless sensors is not possible due to long lifetime requirements and the inability to change batteries, such as embedded in composite panels or concrete structures or on unmanned or robotic space exploration missions.

EXPERIMENTAL SECTION

Preparation of Conductometric Humidity Sensors. Tetrabutyl titanate ($(\text{Ti}(\text{OC}_4\text{H}_9)_4$, >95%), poly(vinylpyrrolidone) (M_w : 1 300 000), and LiCl were purchased from Aldrich and used as received. Square-shaped glass substrates (1 inch × 1 inch) were cut from precleaned glass slides purchased from VWR International. All glassware and glass substrates were cleaned by piranha solution (3:1 (v/v) concentrated sulfuric acid/30% hydrogen peroxide) and dried in a N_2 stream. (Caution: piranha solution is extremely corrosive and can react violently with organic compounds; gloves, goggles, and face shields should be used for protection.) Gold electrodes were deposited on the glass slides by evaporating gold onto the surface using a physical vapor deposition (PVD) method (Figure 1a). A working solution was prepared using the following procedure: 1.5 g of tetrabutyl titanate was mixed with 3 mL of acetic acid and 3 mL of ethanol with continuous stirring.²⁴ The obtained solution was added to 7.5 mL of ethanol containing 0.45 g of poly(vinylpyrrolidone) (PVP) and 0.20 g of LiCl, followed by stirring for 30 min at room temperature. The resulting solution was spin-coated onto glass slides with gold electrodes at a spinning rate of 7000 rpm using an EC101D Photo-resist Spinner Controller (Headway Research Inc.) followed by annealing in a furnace (Lindberg, 58000 series) with a UP150 controller at 520°C for 3 h in order to remove organic components (substrates were placed in a nonsealed quartz tube).

Preparation of SAW Humidity Sensors. The SAW devices fabricated for our measurements were based on SAW-grade YZ- LiNbO_3 (Crystal Technology, Inc.) substrates supporting two closely spaced split electrode Ti/Al transducers at one end of the die and a nonsplit electrode reflector located at the opposite end (Figure 1b). The devices were designed to be measured in a transmission (S21) mode between the two transducers, with the reflector deliberately positioned to produce a reflected response significantly delayed in the time domain so as to not conflict with the multiple-transit responses between the two transducers. The center frequency of the device was designed to be 250 MHz, and the unmatched insertion loss for the direct signal between the two transducers was approximately 12 dB. All of the SAW sensors were O_2 plasma treated (100 mW RF power, 400 mTorr pressure, 50 sccm O_2 flow rate, 1 min) prior to film deposition. Formation of the films on a delay line between the electrodes was performed using the spin coating procedure described above for conductometric sensors. The titanium/aluminum electrodes were covered with adhesive tape during spin coating to avoid deposition of the material onto the electrode area. The tape was removed before annealing.

Characterization of the Films and Measurement of the Sensor Response. The morphology of the films was studied using a

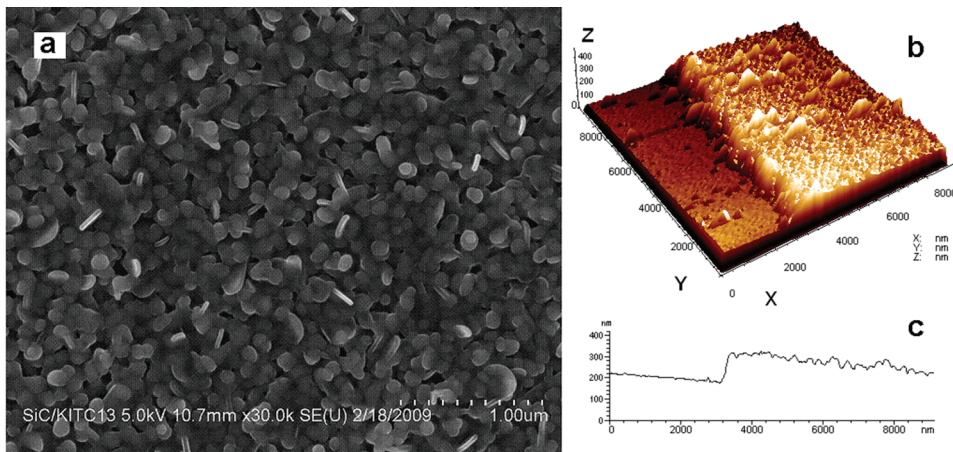


Figure 2. (a) SEM image of TiO_2/LiCl film deposited onto a LiNbO_3 substrate; (b) typical AFM 3D image used to determine film thickness; (c) AFM cross-section showing the profile of the film edge.

scanning electron microscope (SEM, Hitachi S-4800). The X-ray diffraction study was done on a Siemens D500 diffractometer. The transmission Fourier transform infrared spectroscopy (FTIR) study of the film deposited on glass substrate was performed on a Tensor 27 (Bruker) spectrometer before and after annealing. Surface chemical analysis of the material obtained was performed using X-ray photoelectron spectroscopy (XPS, Scienta ESCA 300). Thickness measurements of the films deposited on the SAW substrate were performed using atomic force microscopy (AFM) imaging at a film edge (PicoPlus AFM, Molecular Imaging, Tempe, AZ) with a contact mode silicon nitride AFM tip (NP-S20, force constant 0.12 N/m, Veeco). For these measurements, a razor blade was used to scratch a line, removing a region of the film down to the substrate to produce the required edge. The imaging was done in several randomly chosen spots along the film edge followed by statistical analysis of the data obtained.

Conductivity measurements were performed using a laboratory-made system with a 10 nA/V current amplifier (Molecular Imaging) allowing measurements of low current. Changes in conductivity for the conductometric sensors were recorded for varying humidity levels from 10 to 70% RH, using a wet gas flow obtained by bubbling a N_2 stream through a flask with water, mixed with a dry nitrogen stream. The humidity level was controlled by adjusting the mixing ratio of dry to wet nitrogen flows using a specially designed gas line. Monitoring of the humidity level and temperature in the gas line was performed using an Omega RH32 commercial RH meter.

Characterization of the fabricated SAW sensors was carried out using a RF wafer probe station (Wentworth Laboratories MP-0900) with an Agilent E5070B network analyzer. The sensor signal was measured upon varying humidity from 10 to 70% RH, analogously to the conductometric sensors.

The sensor response dynamics of both types of humidity sensors was characterized against the change in humidity from 5 to 65% using gas mixtures as described above. The response time of the conductometric sensor was measured using a stopwatch, providing the time axis of Figure 3b. The response time measured for the SAW sensors was defined as that required for the response signal to reach 90% of its maximum value, and the recovery time was estimated as that needed for complete recovery of the sensor signal to its initial value when wet nitrogen flow is off. The SAW sensor response data measured by the network analyzer was captured on a computer simultaneously with a computer-generated electronic stopwatch, to allow subsequent frame-by-frame extraction of the time response of the sensor amplitude. Although the time resolution on the stopwatch was 0.1 s, the network analyzer images recorded was only updated every few stopwatch intervals, due to the time required for time domain data generation on the network analyzer.

RESULTS AND DISCUSSION

The strategy of the thin film deposition includes two steps: spin-coating and annealing at high temperature. First, the working solution was prepared (see Experimental Section), and then, PVP was added in order to provide a film-forming matrix for the subsequent spin-coating film deposition step. One of the parameters to consider in order to get a high quality, uniform thin film using a spin-coating process is the viscosity of the solution. Using PVP as a supporting matrix allows partially hydrolyzed $\text{Ti}(\text{OC}_4\text{H}_9)_4$ precursor molecules to be uniformly distributed along the surface of the substrate. Subsequent annealing at 520°C was conducted for 3 h in order to form the TiO_2/LiCl composite and to remove organic components including the PVP matrix and byproducts of the reaction. Such annealing conditions allow complete removal of the organic components and OH bearing species which is confirmed by comparison of the FTIR spectra before and after temperature treatment. (See Supporting Information, Figure 1Sc.) Additional experiments revealed that the annealing process does not lead to any substantial mechanical degradation of the sensor substrates.

Characterization of the Film. The morphology of the films deposited on glass and SAW substrates was studied by SEM (Figure 2a) and was similar in both cases. The morphology of the films consisted of coin-shaped nanoparticles with an average disc thickness of less than 50 nm and disc diameters on the order of several hundred nanometers. The schematic representation of the film formation process shows the initial nanoparticles, consisting of partially hydrolyzed tetrabutyl titanate, distributed in a PVP matrix (see Supporting Information, Figure S1a), which coalesce during the course of the annealing process resulting in larger coin-shaped nanoparticles. (See Supporting Information, Figure S1b.) The absence of features in the XRD spectrum was due to the very small thickness of the film. (The XRD spectrum is not shown.) The surface composition of the obtained material was determined by XPS analysis. The binding energies of the elements revealed formation of TiO_2 in mixture with LiCl (Figure S6, Supporting Information). Increased oxygen content, compared to the theoretically calculated ratio for stoichiometric TiO_2 , can be explained by the presence of the oxygen species (O_2^- , O^{2-} and O^-), chemisorbed on the surface of titanium dioxide due to annealing at 520°C.¹³

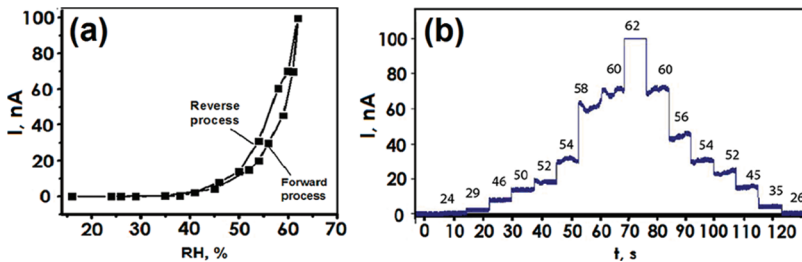


Figure 3. Conductivity measurements of the TiO_2/LiCl film upon relative humidity changes in the region of 13–65 % RH (a); steplike changes with time in the film conductance upon various RH values (numbers on the graph; b).

The thickness estimation was carried out by scratching a film on the SAW substrate with a razor blade to obtain a trench (Figure 2b), followed by AFM imaging at the edge of the trough. (For details on a control experiment see Supporting Information, Figures S3–S5.) A number of images were collected at different spots, and a statistical treatment was performed to estimate average thickness of the film, which was found to be around 140 ± 20 nm. The morphology determined by AFM imaging was in accordance with the data revealed by the SEM study.

Study of Conductometric Sensor Properties. Generally, the films deposited on the gold electrode-supported glass substrates (Figure 1a) exhibited low conductivity with the current being in the nanoampere region (with 10 V bias) at any level of the ambient humidity applied (Figure 3). The films showed reversible electrical changes versus ambient humidity, revealing slight hysteresis (Figure 3a). The current increased as the relative humidity was raised in the measuring chamber, reaching the limit of our preamplifier (100 nA) at 62% RH (Figure 3b). The role of the ionic dopant (LiCl) in the oxide film can be explained within a framework of a model comprehensively described by Qi et al. for the case of TiO_2 nanofibers doped with KCl.²³ In this work, it was proposed that the ionic dopant can dissociate upon water adsorption, creating additional charge carriers which results in a large increase in conductivity at high RH. The data shown herein demonstrates the humidity sensing properties of the film, which exhibit a variation in resistance by two orders of magnitude over a range of humidity of 25–65 % RH with good reversibility. A stopwatch was used to estimate the response time of the conductometric sensors, and it revealed that, for these films, the change in conductivity happens within 0.5 second for a step from 52 to 54 % RH.

Study of the SAW Sensor Response. Motivated by a desire to make a device which could be controlled remotely and wirelessly, the TiO_2 -based film was deposited on SAW device substrates in the acoustic propagation path between the transducers and the reflector, and the sensing properties of the resulting SAW devices were measured at varying humidity levels (Figure 4, see also Supporting Information, Figure S7). Strong, rapid, and fully reversible SAW signal variations were clearly observed with changing humidity levels. It is seen that the SAW response drops by more than 60 dB over the whole RH range applied (Figure 4). The large change in the amplitude of the SAW at higher humidity levels may be partially due to mass loading or to viscoelastic effects such as changes in shear loss modulus (G) of the film. However, another parameter which appears to have a significant influence on the SAW properties of the studied sensor is the change in film conductivity upon exposure to varying RH. It is

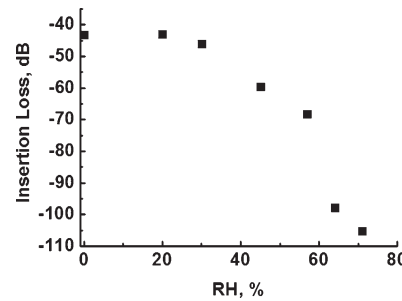


Figure 4. Variation in the SAW device insertion loss (dB) versus ambient relative humidity.

well known that, for electrically conductive coatings on SAW devices, as film conductivity ranges from short circuited (perfect conductor) to open circuit (perfect insulator), the SAW velocity increases monotonically and the SAW attenuation exhibits a peak at the conductivity corresponding to the value at which the velocity is changing most rapidly with changes in conductivity, where the maximum attenuation can exceed $10 \text{ dB}/\lambda$.^{34–36} Conductivity measurements revealed that the studied film exhibits a large increase in conductivity, over two orders of magnitude over the RH range evaluated. As these films are highly resistive as deposited (over $100 \text{ M}\Omega$), this large increase in conductivity can be a partial explanation of the substantial SAW attenuation change over the same RH range. In order to understand comprehensively the origin of the observed SAW properties of the studied TiO_2 -based film as a function of RH and to build a theoretical model to account for this, further detailed study needs to be carried out to separate the effects of conductivity from those of mass loading and film viscoelastic properties.

The studied SAW sensor exhibits the greatest signal variation at RH levels between 20% and 65%. Above 70% RH, the sensor response hit the noise floor of the measurement system. A reduction of sensor device insertion loss would allow the operating range of these devices to extend to higher RH levels. Also, while changes in sensor performance at RH levels below 20% appear small on a dB scale, one should recognize that, since the sensor signal is much larger at the low insertion loss levels observed for low RH levels, these changes actually correspond to significant, measurable changes in the linear signal amplitude. These results indicate that modification of the film thickness can be used in conjunction with device design to tailor sensor properties to optimize performance for the RH range(s) relevant to specific application(s). Some preliminary results, conducted in our laboratory, have already shown the validity of this approach.

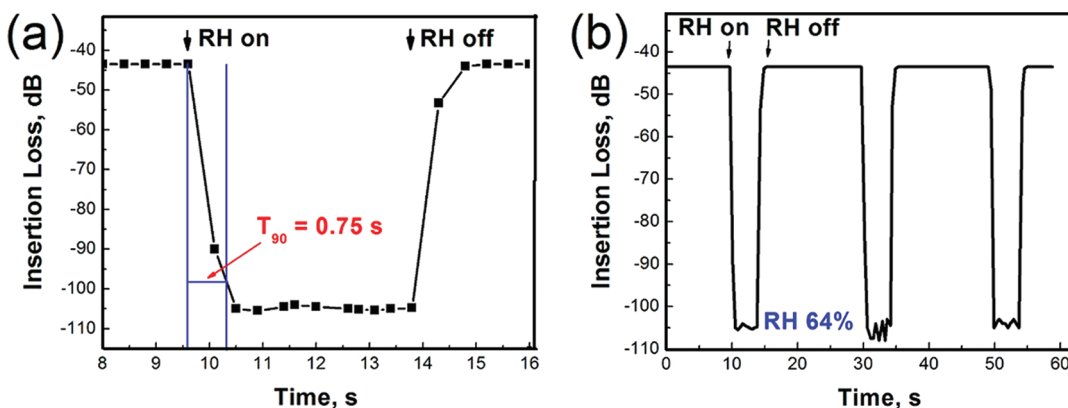


Figure 5. LiCl doped TiO_2 nanomaterial film SAW response dynamics to 64% RH (a); repeatability of the sensor response (b).

Unlike published results for SAW humidity sensors, where responses take many seconds to minutes,^{37–40} the changes in the response of the SAW sensor device described here were found to occur in less than a second. In order to evaluate the speed of sensor response and recovery, as well as sensor response reproducibility, repeated humidity exposure measurements at set humidity levels were conducted. Even with the limited time resolution of the network analyzer as described above, the response time can be measured on the order of fractions of a second. The response time, t_{90} , of the sensor upon a jump in humidity from 5 to 64% RH is around 0.75 s, and it takes less than 1 s for a complete recovery of the signal, as shown in Figure 5a (see also Figure S2, Supporting Information). The actual response time of the sensor may be faster than observed since our humidity generating apparatus limits the rate at which we can change the humidity of the test environment of the sensor, and this humidity jump is not instantaneous. The sensor exhibits a repeatable response as shown in Figure 5b for several cycles of exposure. Comparison to the literature data^{37–40} shows that the response dynamics of the sensor obtained in our work appears to be among the fastest reported SAW humidity sensors. In addition, the relatively simple deposition procedure, without the use of expensive deposition equipment (physical vapor deposition (PVD), chemical vapor deposition (CVD)), is an additional feature making these devices promising for low cost, high volume production.

The synthetic approach used in this paper is based on the work of Li et al. where 1D nanofibers were successfully obtained by electrospinning.²⁴ Li et al. considered the advantages of the 1D nanostructure over 2D films in terms of sensor sensitivity and found generally better performance of the former when it comes to humidity detection.²⁴ The advantages of 1D nanofibers include facilitated fast mass transfer of the water molecules toward and away from the interaction region, as well as greatly reduced interfacial areas between the active sensing region of the nanofibers and the underlying substrate, all leading to a better sensor performance. Besides, elongated 1D nanofibers have fewer interparticle contacts. All the above features undoubtedly appear to be advantageous in conductometric type humidity sensors, when either change in conductivity/resistance or change in impedance is measured as a sensor response. However, when it comes to SAW sensor devices, utilization of uniform 2D nanostructured films, in our opinion, leads to better sensor operation in terms of sensitivity and response time, compared to 1D nanostructures, e.g., nanofibers. This assessment is based on the fact that the influence of the surface condition on the propagating

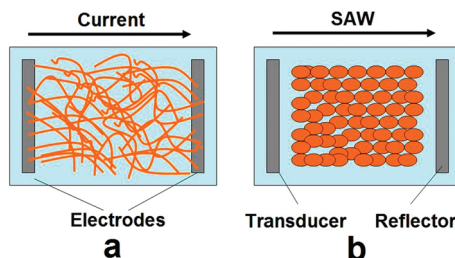


Figure 6. Utilization of different film morphologies for different sensor types: (a) conductometric/resistance type sensors; (b) SAW sensors.

surface acoustic wave depends on the number of particles and the particle surface area per unit area interacting with the electro-mechanical wave. Clearly, in 2D films, the density of the TiO_2 /LiCl sensor material per unit surface area in the wave propagation region is much higher compared to a similar film consisting of interlaced 1D nanofibers (as shown, for example, in Figure 1, Li et al.²⁴). The results of this work indicate that the deposition of a thin uniform 2D film consisting of nanoparticles with low size distribution provides desirable sensor performance, producing SAW sensor devices with both high sensitivity and rapid responses. Small, closely packed nanoparticles, forming a 2D film, provide a higher density of material while still providing significant surface area for interactions (Figure 6b). This means that the effect on SAW propagation of mass loading or visco-elastic changes will be greater than that produced by a film consisting of nanofibers, while the magnitude of conductivity induced changes will depend on the conductivity of the films relative to the peak of attenuation vs. conductivity for the SAW sensor substrate utilized (Figure 6a).

In light of the above considerations, we made a substantial modification to the strategy of the synthetic approach, described earlier.²⁴ The electrospinning deposition step which leads to 1D nanofibers was substituted with spin coating of the working solution and subsequent annealing as described above, which led to the formation of the 2D morphology described in this work.

CONCLUSIONS

A spin-coating procedure was implemented to deposit TiO_2 /LiCl-based conducting thin films on the surface of glass and LiNbO_3 substrates. SEM observation of the films revealed formation of coin-shaped nanoparticles. The sensing characteristics of the fabricated conductometric and SAW sensors towards humidity

were studied, revealing rapidly responding humidity devices. Conductance variation of the conductometric sensor by two orders of magnitude upon exposure to 65% RH was recorded to occur in less than 0.5 s. Corresponding humidity exposure tests with the obtained SAW sensor revealed SAW responses varying in a 70 dB range over the RH range of 5–95%. The dynamic characteristics of the SAW humidity sensor were found to be 0.75 and 1 s for sensor response and recovery, respectively. Repeated humidity cycling tests demonstrated stable device operation and high repeatability of sensor response. Thus, a simple and straightforward way of fabricating nanostructured thin films, based on LiCl doped TiO₂, was demonstrated without the use of expensive CVD or PVD equipment. The applicability of the obtained film for creating conductometric and SAW humidity sensors was shown. The rapid, responsive SAW humidity sensor designed in this work can be utilized for wireless remote data acquisition and appears to be beneficial for applications in situations when real time humidity measurement and data acquisition in difficult to access places is needed.

■ ASSOCIATED CONTENT

Supporting Information. Illustration of the sensor response time measurements; control experiment for the film thickness measurements by AFM; XPS data. This material is available free of charge via the Internet at <http://pubs.acs.org>.

■ AUTHOR INFORMATION

Corresponding Author

*Address: Department of Chemistry, 130 Beury Hall, Temple University, 1901 N 13th Street, Philadelphia, PA 19122. Phone: 215-204-9696. Fax: 215-204-9530. E-mail: eborguet@temple.edu.

■ ACKNOWLEDGMENT

The authors acknowledge generous support by NASA Contract NNX08CD42P. The assistance of Dr. Andrew Randles in fabricating the SAW sensors and in measuring SAW sensor responses and Sally Shrom in obtaining SEM images is appreciatively acknowledged. The XPS spectra were recorded at Lehigh University by Dr. Alfred Miller, whose assistance is gratefully acknowledged as well as assistance of Dr. Doug Hausner from Temple University in processing XPS data.

■ REFERENCES

- (1) Venugopalan, T.; Yeo, T. L.; Sun, T.; Grattan, K. T. V. *IEEE Sens. J.* **2008**, *8*, 1093–1098.
- (2) Luechinger, N. A.; Loher, S.; Athanassiou, E. K.; Grass, R. N.; Stark, W. J. *Langmuir* **2007**, *23*, 3473–3477.
- (3) Zhang, N.; Yu, K.; Zhu, Z. Q.; Jiang, D. S. *Sens. Actuators, A* **2008**, *143* (2), 245–250.
- (4) Yamazoe, N.; Shimizu, Y. *Sens. Actuators, B* **1986**, *10*, 379–398.
- (5) Rittersma, Z. M. *Sens. Actuators, A* **2002**, *96*, 196–210.
- (6) Li, Y.; Yang, M. J. *Sens. Actuators, B* **2002**, *86*, 155–159.
- (7) http://www.ist-ag.com/eh/ist-ag/resource.nsf/imgref/Download_270809_P14_Rapid_EN_V4.3.pdf.
- (8) Tetelin, A.; Pellet, C.; Laville, C.; N'Kaoua, G. *Sens. Actuators, B* **2003**, *91*, 211–218.
- (9) Wilson, W. C.; Malocha, D. C.; Kozlofski, N.; Gallagher, D. R.; Fisher, B.; Pavlina, J.; Saldanha, N.; Puccio, D.; Atkinson, G. M. *IEEE Sens. J.* **2009**, *9* (11), 1546–1556.
- (10) Chen, Z.; Lu, C. *Sens. Lett.* **2005**, *3*, 274–295.

- (11) Sun, A. H.; Huang, L.; Li, Y. *Sens. Actuators, B* **2009**, *139*, 543–547.
- (12) Tai, W. P.; Oh, J. H. *Sens. Actuators, B* **2002**, *85*, 154–157.
- (13) Qi, Q.; Feng, Y. L.; Zhang, T.; Zheng, X. J.; Lu, G. Y. *Sens. Actuators, B* **2009**, *139*, 611–617.
- (14) Hoyt, A. E.; Ricco, A. J.; Bartholomew, J. W.; Osbourn, G. C. *Anal. Chem.* **1998**, *70*, 2137–2145.
- (15) Faia, P. M.; Furtado, C. S.; Ferreira, A. J. *Sens. Actuators, B* **2004**, *101*, 183–190.
- (16) Agarwal, S.; Sharma, G. L. *Sens. Actuators, B* **2002**, *85*, 205–211.
- (17) Steele, J. J.; Taschuk, M. T.; Brett, M. J. *IEEE Sens. J.* **2008**, *8*, 1422–1429.
- (18) Steele, J. J.; Gospodyn, J. P.; Sit, J. C.; Brett, M. J. *IEEE Sens. J.* **2006**, *6*, 24–27.
- (19) Wang, G.; Wang, Q.; Lu, W.; Li, J. H. *J. Phys. Chem. B* **2006**, *110*, 22029–22034.
- (20) Qi, Q.; Zhang, T.; Yu, Q. J.; Wang, R.; Zeng, Y.; Liu, L.; Yang, H. B. *Sens. Actuators, B* **2008**, *133*, 638–643.
- (21) Montesperelli, G.; Pumo, A.; Traversa, E.; Gusmano, G.; Bearzotti, A.; Montenero, A.; Gnappi, G. *Sens. Actuators, B* **1995**, *25*, 705–709.
- (22) Baraton, M. I.; Merhari, L. *J. Eur. Ceram. Soc.* **2004**, *24*, 1399–1404.
- (23) Qi, Q.; Zhang, T.; Wang, L. *J. Appl. Phys. Lett.* **2008**, *93*, 277–283.
- (24) Li, Z. Y.; Zhang, H. N.; Zheng, W.; Wang, W.; Huang, H. M.; Wang, C.; MacDiarmid, A. G.; Wei, Y. *J. Am. Chem. Soc.* **2008**, *130*, 5036–5037.
- (25) Kuang, Q.; Lao, C. S.; Wang, Z. L.; Xie, Z. X.; Zheng, L. S. *J. Am. Chem. Soc.* **2007**, *129*, 6070–6071.
- (26) Wu, R. J.; Sun, Y. L.; Lin, C. C.; Chen, H. W.; Chavali, M. *Sens. Actuators, B* **2006**, *115*, 198–204.
- (27) Zhang, Y. S.; Yu, K.; Jiang, D. S.; Zhu, Z. Q.; Geng, H. R.; Luo, L. Q. *Appl. Surf. Sci.* **2005**, *242*, 212–217.
- (28) Wang, X. H.; Zhang, J.; Zhu, Z. Q.; Zhu, J. Z. *Appl. Surf. Sci.* **2007**, *253*, 3168–3173.
- (29) Krishnakumar, T.; Jayaprakash, R.; Singh, V.N.; Mehta, B.R.; Phani, A.R. *J. Nano Res.* **2009**, *4*, 91–101.
- (30) Chou, K.-S.; Lee, T.-K.; Liu, F.-J. *Sens. Actuators, B* **1999**, *56*, 106–111.
- (31) Radeva, E. I.; Martev, I. N.; Dechev, D. A.; Ivanov, N.; Tsaneva, V. N.; Barber, Z. H. *Surf. Coat. Technol.* **2006**, *201*, 2226–2229.
- (32) Lee, E. T.; Jang, G.E.; Kim, C.K.; Yoon, D.H. *Sens. Actuators, B* **2001**, *77*, 221–227.
- (33) Steele, J. J.; Fitzpatrick, G. A.; Brett, M. J. *IEEE Sens. J.* **2007**, *7*, 955–956.
- (34) Auld, B. A.; Wilson, D. A.; Winslow, D. K.; Young, E. *Appl. Phys. Lett.* **1971**, *18*, 339–341.
- (35) Hemphill, R. B. Effect of a Thin-Film Phase-Transition Material on Surface Acoustic Wave Propagation. In *IEEE 1984 Ultrasonics Symposium Proceedings*; IEEE: New York, 1984; pp 1006–1010.
- (36) Hemphill, R. B. Attenuation of Acoustic Waves on a Piezoelectric Coated with Thin Metal Films. In *1972 Ultrasonics Symposium Proceedings*; IEEE: Boston, 1972; pp 340–342.
- (37) Wu, T. T.; Chen, Y. Y.; Chou, T. H. *J. Phys. D* **2008**, *41*, 3231–3235.
- (38) Chen, Y. T.; Kao, H. L. *Electron. Lett.* **2006**, *42*, 948–950.
- (39) Penza, M.; Cassano, G. *Sens. Actuators, B* **2000**, *68*, 300–306.
- (40) Penza, M.; Anisimkin, V. I. *Sens. Actuators B: Chem.* **1999**, *76*, 162–166.